EUROPEAN ORGANIZATION FOR NUCLEAR RESEARCH

CERN/EP 79-58
15 June 1979

CROSS SECTIONS AND MULTIPLICITY DISTRIBUTIONS FOR K^+p INTERACTIONS AT 70 GeV/c

M. Barth, C. De Clercq, E. De Wolf(*), J.J. Dumont, M. Gijsen, D.P. Johnson, J. Lemonne and P. Peeters
Inter-Univ. Inst. f. High Energies, (ULB-VUB), Brussels, Belgium

H. Drevermann, Y. Goldschmidt-Clermont, G. Harigel, J.P. Porte, R.T. Ross and A. Stergiou
CERN, European Organization for Nuclear Research, Geneva, Switzerland

C. Caso, R. Contri, R. Monge, S. Squarcia and U. Trevisan
Sezione INFN and Istituto di Scienze Fisiche, Genova, Italy

J.F. Baland, J. Beaufays, F. Grard and J. Kesteman
Faculté de Science, Université de l'Etat, Mons, Belgium

P.A. van der Poel, W. Kittel, W.J. Metzger, D.J. Schotanus and R.T. Van de Walle
University of Nijmegen, Nijmegen, Netherlands(**)

Y.A. Belokopitov, P.V. Chliapnikov, A.B. Fenyuk, S.V. Klimenko, V.M. Kubic, S.B. Lugovsky, V.N. Nikolaenko, Y.L. Petrovikh, V.M. Ronjin, A.P. Vorobjev and V.A. Yarba
Inst. for High Energy Physics, Serpukhov, USSR(***)

G. Alexander, S. Dagan, D. Lissauer and C. Milstene
University of Tel-Aviv, Tel-Aviv, Israel

Submitted to Zeitschrift für Physik C Particles and Fields

(*) Bevoegdverklaard Navorser, NFWO Belgium; also at the Universitaire Instelling, Antwerpen, Belgium

(**) Supported in part by the joint ZWO-FOM research program.

(***) Participating under the terms of the 1967 Agreement between CERN and the USSR State Committee for the Utilisation of Atomic Energy and the Protocols thereto.

CC/mk

ABSTRACT

Cross sections and charged multiplicity distributions for K^+p interactions at 70 GeV/c are presented and compared with K^+p data at other energies.

Comparisons are also made with available π^+p, pp and K^-p data.

We present results on topological cross sections and charged-particle multiplicities for 70 GeV/c K^+p interactions from the hydrogen filled BEBC bubble chamber in CERN exposed to a r.f. separated beam of positive kaons [1]. The nominal beam momentum was 70 GeV/c at the bubble chamber with a momentum spread of ± 0.25%.

Using the information from the Cerenkov counters upstream of the bubble chamber and from the scanning of beam-like incident tracks on pictures with the r.f. turned off, the π- and μ-contaminations were determined to be $\sim$ 2% and $\sim$ 1% respectively. The hydrogen density was (0.0620 ± 0.0008) g/cm^3 as determined by measuring the chamber operating conditions during the run. The chamber was used in a double-pulsing mode in alternating exposure with a wide-band neutrino beam.

As a first step, some 42 000 pictures were taken; the aperture of the upstream Cerenkov counters (used for checking purposes in this first run) limited the possible horizontal spread of the beam. As a result, the mean number of incident particles had to be kept relatively low ($\sim$ 4 per picture) yielding $\sim$ 0.5 interactions per hadronic frame in the fiducial volume.

The results presented here come from a first sample of $\sim$ 28 000 pictures corresponding to $\sim$ 0.73 events/μb. These pictures were scanned twice using a fiducial length of (200 ± 2) cm. This allows an incident track length of at least 0.7 m and a minimum secondary track length greater than one meter.

The differences in the two independent scans were resolved at the scanning table, yielding a $\sim$ 85% scanning efficiency for 2-prong interactions and $\sim$ 100% for all other topologies. Further losses of 2-prong events are discussed below.

The scanning results were corrected for wrong topology assignments in the following way:

(a) Odd pronged events were carefully examined in four views with the maximum available magnification. Three-prong events were corrected for the

expected number of τ-decays. The few remaining unresolvable cases (∿ 1.2%) were distributed among the neighbouring even topologies proportionally to the number of events found in those categories.

(b) The detected electrons and apparent Dalitz-pair tracks were included in the prong counts. The empirical rule $\langle n_{\pi^0} \rangle = \langle n_- \rangle + 0.4$ [2] (where $\langle n_- \rangle$ is the average number of produced negative particles) was used to calculate the expected number of Dalitz-pairs. They were then distributed over the different topologies proportionally to the observed number of gammas for that topology. A comparison was made between the expected and the observed number of Dalitz-pairs for a partial sample. The agreement was very satisfactory, indicating that the empirical rule for π^0 production is well satisfied.

(c) Corrections for V^0's and gammas occurring close to the primary vertex were evaluated for each topology by extrapolating to zero the distributions of the distance between the primary and the neutral vertices. Subsequently, appropriate topology-dependent correction factors were applied to reduce the charged multiplicities.

From a partial sample of 12 450 measured events, containing 2055 2-prongs, a subsample was extracted having tracks compatible with a proton and a kaon mass assignment. From these 909 elastic events were selected with a combined cut on the missing-mass squared and the coplanarity. The loss of elastic events was calculated as follows: the differential cross section $d\sigma/dt$ was fitted in the range $.20 \leqslant t \leqslant .56$ $(GeV)^2$ by a simple exponential law, giving a slope of $(7.91 \pm .20)$ GeV^{-2}.

This value is in quite good agreement with that obtained by Ayres et al. [3] and our data are equally well described by the quadratic exponential form used by these authors $d\sigma/dt \sim \exp(-8.1t + 2.2t^2)$. The extrapolation to $t = 0$ using the constraint given by the optical theorem gives an overall loss of (40.4 ± 2.5)% of elastic events. Finally, no azimuthal correction was found to be necessary for 2-prong inelastic events.

Taking into account all these corrections and using the total effective beam length as determined from beam track counting and the beam attentuation, we obtained a value of (18.60 ± .17)mb for the total cross section. This value is somewhat larger than the value σ_{tot} = (18.36 ± .09)mb obtained in a counter experiment [3]. We attribute this to the difficulty of a clear scanning definition of beam tracks at this energy. For this reason, we prefer to normalize our topological cross sections to the value of ref. [3]. Our results are given in table 1 and displayed in fig. 1 together with results obtained at other energies [4]. The curves are drawn only to guide the eye. In general, our 70 GeV/c data interpolate smoothly between the values obtained at lower momenta and those obtained at 100 and 147 GeV/c. Some anomalies appearing at 100 GeV/c are probably due to the very limited statistics of that experiment. At 70 GeV/c all topologies up to n = 10 have cross sections larger than 1 mb. The 2- and 4-prong cross sections are decreasing in roughly the same way.

We have calculated various charged multiplicity parameters both for all tracks and for the negative tracks only and listed the values in table 2. In general, our numbers interpolate in a satisfactory way between the results obtained at other momenta; this is shown explicitly in figs 2 and 3 in which data collected in a momentum range from 3 to 147 GeV/c are used.

An attempt to fit the average charge multiplicity $\langle n_c \rangle$ as a function of s, assuming either linear ln s dependence or a simple power law, yielded very poor χ^2/ND values ($\gtrsim$ 5). Similar conclusions were reached in the experiment at 147 GeV/c [4].

A good description was obtained by fitting the expressions

$$\langle n_c \rangle = a + b \ln s + c s^{-\frac{1}{2}} + d s^{-\frac{1}{2}} \ln s \qquad (1)$$

$$\langle n_c \rangle = a + b \ln s + c (\ln s)^2 \qquad (1')$$

to the data. The former expression is preferred on theoretical grounds

(Mueller-Regge approach; see ref. [5]) while the latter was found to give a good description of pp and K^-p data at high energies [6]. The resulting parameters are given in table 3; these should be treated with caution because they are highly correlated. The fitted curves are superimposed on the data in fig. 2, where it is evident that up to presently available energies both parametrizations describe the K^+p data equally well.

The dependence of the dispersion D on $\langle n_c \rangle$ is shown in fig. 3. The trend of the data agrees with the so-called Wroblewski rule [7], namely with a linear behaviour

$$D = a \langle n_c \rangle + b. \qquad (2)$$

For b we find $-.45 \pm .02$.

A value of b different from zero implies a deviation from exact KNO scaling [8], which requires that $C_k = \langle n_c^k \rangle / \langle n_c \rangle^k$, and hence $\sqrt[k]{\mu_k}/\langle n_c \rangle$ (see table 2 for definitions), must be constant with energy. However, a scaling law may be formulated [9] in terms of a modified KNO function $\psi(z)$ with

$$z = \frac{n_c - \alpha}{\langle n_c \rangle - \alpha} \quad \text{where } \alpha = -\frac{b}{a} \ . \qquad (3)$$

Clearly, this procedure allows a very good description of the data. The curve

$$\psi(z) = \frac{3.333\ z}{\left[\Gamma(z+1)\right]^2} \exp(-.892\ z) \qquad (4)$$

derived in ref. [10] is superimposed on K^+p data at all available energies in fig. 4(a). In addition, it is interesting to present our data according to the method proposed by Czyżewski and Rybicki [11]. Their prescription is to plot the variable $D \cdot P(n_c) = D \cdot \sigma_n/\sigma_{inel}$ versus $(n_c - \langle n_c \rangle)/D$;

a good fit is then obtained for data at all available energies in terms of a generalized one-parameter Poisson distribution. Fig. 4(b) shows the remarkable agreement between the data and the prediction. It is interesting to compare the K^+ results at high energies with data from other positive incident particles in the same energy range, namely protons from 19 to 205 GeV/c and pions from 18.5 to 147 GeV/c. Fig. 5 shows the behaviour of the average charge multiplicity $\langle n_c \rangle$. The π^+ averages are consistently higher than the proton data points, while the K^+ data lie somewhere in between. A similar phenomenon observed for different processes at much lower energies [12] was interpreted as an additive quantum number (charge, baryon number, strangeness) conservation effect.

The π^+ versus proton effect has been already studied in several papers (see for example ref. [13]) in terms of independent quark models. The simplest model assumes that single quark-quark interactions are the predominant mechanism for producing secondary particles and that the available momentum is equally shared between the valence quarks in the colliding particles. A constant difference $\langle n_c \rangle_{\pi^+} - \langle n_c \rangle_p = 0.7$ is then inferred and this value is in good agreement with the low energy data. At high energies a new mechanism seems to contribute because all the valence quarks can be involved in the interaction. On this basis an asymptotic value of $\langle n_c \rangle_{\pi^+} - \langle n_c \rangle_p = 0.33$ was derived. The data can then be explained by assuming a progressive onset of this latter mechanism. A different analysis [14] using a perturbative Reggeon calculation in which differences in absorption are taken into account, predicts that the $\langle n_c \rangle_p$ data should crossover the $\langle n_c \rangle_{\pi^+}$ data at c.m. energies as high as 10^3 GeV^2. The experimental data show that the difference appears clearly to decrease with increasing energy, but it is still impossible to say whether such a crossover occurs or an asymptotic non zero difference will be reached. On the basis of the same quark models and naively neglecting effects due to the more massive strange quark in the kaon, one would expect $\langle n_c \rangle_{K^+}$ to be nearly equal to $\langle n_c \rangle_{\pi^+}$ as a function of energy. This is not observed in our data: the K^+ versus p effect is smaller. It was already shown that one is not justified in assuming the

equidistribution of momentum between the two quarks of the kaon. It is difficult at this point to decide which part of the difference $\langle n_c \rangle_{K^+} - \langle n_c \rangle_p$ (or alternatively $\langle n_c \rangle_{K^+} - \langle n_c \rangle_{\pi^+}$) is due to the strange quark and which to the energy dependence.

From eq. (2) one would expect also a difference between the dispersions $D(\pi^+)$, $D(K^+)$ and $D(p)$. No such effect appears in the behaviour of D, also shown in fig. 5. It follows that the straight lines D vs $\langle n_c \rangle$ must have different intercepts for different incident particles i.e. that KNO scaling violation depends on the type of incident particle. Practically the same conclusions about KNO-scaling violation can be derived from an inspection of fig. 6 where the energy dependence of the second normalized moment C_2 is displayed, both for all charged and for negative secondary particles only. Higher moments (not shown) behave in a similar way, their relative variation with increasing energy becoming greater as the order of the moment increases.

We turn now to discuss the skewness (γ_1) and kurtosis (γ_2) parameters (see definitions in table 2). In figs 7 and 8, γ_1 and γ_2 are plotted both for K^+ and K^- data and for all available energies. A different behaviour of the two sets of points is observed. The differences at lower energies disappear as soon as the zero-prong cross section is removed from K^- data.

The asymptotic values

$$\gamma_1 = 2/3 \qquad \gamma_2 = 3.2$$

already observed for other incident particles [15] are also reached in $K^{\pm}p$ interactions.

Finally we consider the Mueller correlation coefficient

$$f_2 = D^2 - \langle n_c \rangle \ . \tag{5}$$

Fig. 9 shows f_2^{cc}, while f_2^{--} is plotted in fig. 10. Again it is of

interest to compare K^+ and K^- data. Due to the linear dependence of D on $\langle n_c \rangle$, one should expect a non-constant behaviour for f^{cc} indicating a progressive broadening of the charge multiplicity distribution. There is a significant deviation from Poisson-like multiplicity behaviour both below $s \sim 40$ GeV^2 and above $s \sim 100$ GeV^2. The curve superimposed on the data of fig. 9 is the prediction from the fit in fig. 3. The differences between K^+ and K^- at low energies are due to the zero-prong events in K^-p interactions which result in a lower $\langle n_c \rangle$ and in a multiplicity distribution which is wider below the mean value, giving a larger D. The differences disappear at high energies when the relative contribution of the zero-prong cross section becomes less important.

The behaviour of f_2^{--} in fig. 10 is similar. Despite its low values, f_2^{--} is significantly different from zero (except in the 150-200 GeV^2 region).

Acknowledgements

It is a pleasure to thank the scanners of our respective laboratories, as well as the operating crews of BEBC and the accelerator.

REFERENCES

[1] H. Atherton et al., CERN/D.Ph.II/BEAM 73-5.

[2] A. Wroblewski, Review of experimental data on multiparticle hadronic reactions, Kaysersberg, June 1977.

[3] D.S. Ayres et al., Phys. Rev. D15 (1977) 3105.

[4] J. Whitmore, Phys. Report 10C (1974) 273;
J. Whitmore, Phys. Report 27C (1976) 187;
D. Brick et al., Topological cross sections for K^+p interactions at 147 GeV/c, submitted to the XIX International Conference on High Energy Physics, Tokyo, Japan, 23-31 August 1978.

[5] P. Chliapnikov et al., Sov. Journ. Nucl. Phys. 26 (1977) 153.

[6] W. Thomé et al., Nucl. Phys. B129 (1977) 365.

[7] A. Wroblewski, Proceedings of the 3rd International Colloquium on Multiparticle Reactions, Zakopane 1972, page 140.

[8] Z. Koba et al., Nucl. Phys. B40 (1972) 317.

[9] A.J. Buras et al., Phys. Lett. 47B (1973) 251;
R. Møller, Nucl. Phys. 74B (1974) 145.

[10] E.H. de Groot, Phys. Lett. 57B (1975) 159.

[11] O. Czyżewski and V.K. Rybicki, Nucl. Phys. B47 (1972) 633.

[12] C. De Clercq et al., to be published in Phys. Rev. D.

[13] W.M. Morse et al., Phys. Rev. D15 (1977) 66;
M.A. Cirit, Phys. Lett. 82B (1979) 123 and references therein.

[14] C. Pajares and R. Pascual, Nucl. Phys. B137 (1978) 390.

[15] E. De Wolf et al., Nucl. Phys. B87 (1975) 325.

TABLE CAPTIONS

Table 1 Topological cross sections for K^+p interactions at 70 GeV/c.

Table 2 Parameters of the charged multiplicity distributions for 70 GeV/c K^+p.

Table 3 Parameters of the fits of the average charged multiplicity as a function of s.

TABLE 1

Topology	Uncorrected Number of events	Cross sections (mb) (a)
2-prongs total	2105	4.17 ± .16
2-prongs elastic		2.36 ± .14
2-prongs inelastic		1.81 ± .07
4-prongs	3342	4.44 ± .09
6-prongs	3226	4.24 ± .09
8-prongs	2353	3.01 ± .07
10-prongs	1324	1.67 ± .05
12-prongs	501	.58 ± .03
14-prongs	155	.18 ± .02
16-prongs	44	.05 ± .01
18-prongs	12	.015 ± .005
20-prongs	1	.0013 ± .0013
Total	13 063	18.36 ± .09

(a) Normalized to the σ-total value of ref. [3]

TABLE 2

	All charged tracks	Neg. charged tracks only
$\langle n_c \rangle$	6.14 ± .03	2.07 ± .02
$\langle n_c^2 \rangle$	45.48 ± .44	6.23 ± .08
$\langle n_c(n_c - 1) \rangle$	39.34 ± .41	4.16 ± .07
D (a)	2.80 ± .02	1.40 ± .01
$\langle n_c \rangle / D$	2.20 ± .02	1.48 ± .01
f_2 (b)	1.68 ± .12	-.12 ± .03
f_3 (c)	2.90 ± .59	.03 ± .07
μ_3 (d)	14.06 ± .81	1.76 ± .10
$\gamma_1 = \mu_3/D^3$ (d)	.64 ± .03	.64 ± .03
$\gamma_2 = \mu_4/D^4$ (d)	3.30 ± .09	3.30 ± .09
$C_2 = \langle n_c^2 \rangle / \langle n_c \rangle^2$	1.207 ± .003	1.456 ± .008
$C_3 = \langle n_c^3 \rangle / \langle n_c \rangle^3$	1.68 ± .01	2.57 ± .04
$C_4 = \langle n_c^4 \rangle / \langle n_c \rangle^4$	2.63 ± .04	5.22 ± .13

(a) $D = (\langle n_c^2 \rangle - \langle n_c \rangle^2)^{\frac{1}{2}}$.

(b) $f_2 = \langle n_c(n_c - 1) \rangle - \langle n_c \rangle^2 = D^2 - \langle n_c \rangle$.

(c) $f_3 = \langle n_c(n_c - 1)(n_c - 2) \rangle - 3 \langle n_c(n_c - 1) \rangle \langle n_c \rangle + 2 \langle n_c \rangle^3$.

(d) $\mu_i = \langle (n_c - \langle n_c \rangle)^i \rangle$.

TABLE 3

Parameters	Fit (1)	Fit (1')
a	-3.80 ± 2.14	1.32 ± 0.10
b	1.87 ± 0.29	0.40 ± 0.07
c	5.77 ± 1.25	0.12 ± 0.01
d	0.74 ± 1.54	-
χ^2/ND	.6	.7

FIGURE CAPTIONS

Fig. 1 The topological cross sections in K^+p interactions, as a function of $\sqrt{s}$. The hand-drawn curves are only intended to guide the eye.

Fig. 2 The average charged multiplicity as a function of s for all available K^+ data. The two curves refer to the fits described in the text (dashed line: fit (1); solid line: fit (1')). The parameter values are given in table 3.

Fig. 3 The dispersion as a function of the average charged multiplicity for K^+p interactions.

Fig. 4 Comparison between data and modified multiplicity distributions for K^+p interactions:

(a) $[\langle n_c \rangle - \alpha]\ \sigma_n/\sigma_{inel}$ vs $z = (n_c - \alpha)/(\langle n_c \rangle - \alpha)$. The curve is taken from ref. [10].

(b) $D\ \sigma_n/\sigma_{inel}$ vs $[n_c - \langle n_c \rangle]/D$. The curve is taken from ref. [11], with d = 1.8.

Fig. 5 The average charged multiplicity and the dispersion for high energy ($\gtrsim$ 20 GeV/c)pp, π^+p and K^+p interactions plotted as a function of s.

Fig. 6 Energy dependence of $\langle n_c^2 \rangle / \langle n_c \rangle^2$ for all charged tracks and for negative tracks.

Fig. 7 Energy dependence of the skewness γ_1 of the multiplicity distribution. Data from K^+p and K^-p interactions are compared. The dashed line represents the asymptotic value $\gamma_1 = 2/3$ [15].

FIGURE CAPTIONS (Cont'd)

Fig. 8 Comparison between the kurtosis γ_2 of K^+ and K^- multiplicity distributions. The value $\gamma_2 = 3.2$ (dashed line) is suggested in ref. [15].

Fig. 9 The correlation parameter f_2^{cc} as a function of s, both for K^+ and K^- induced reactions. The dashed line is the result predicted from the linear fit of fig. 3.

Fig. 10 The correlation parameter f_2^{--} for negative particles as a function of s.

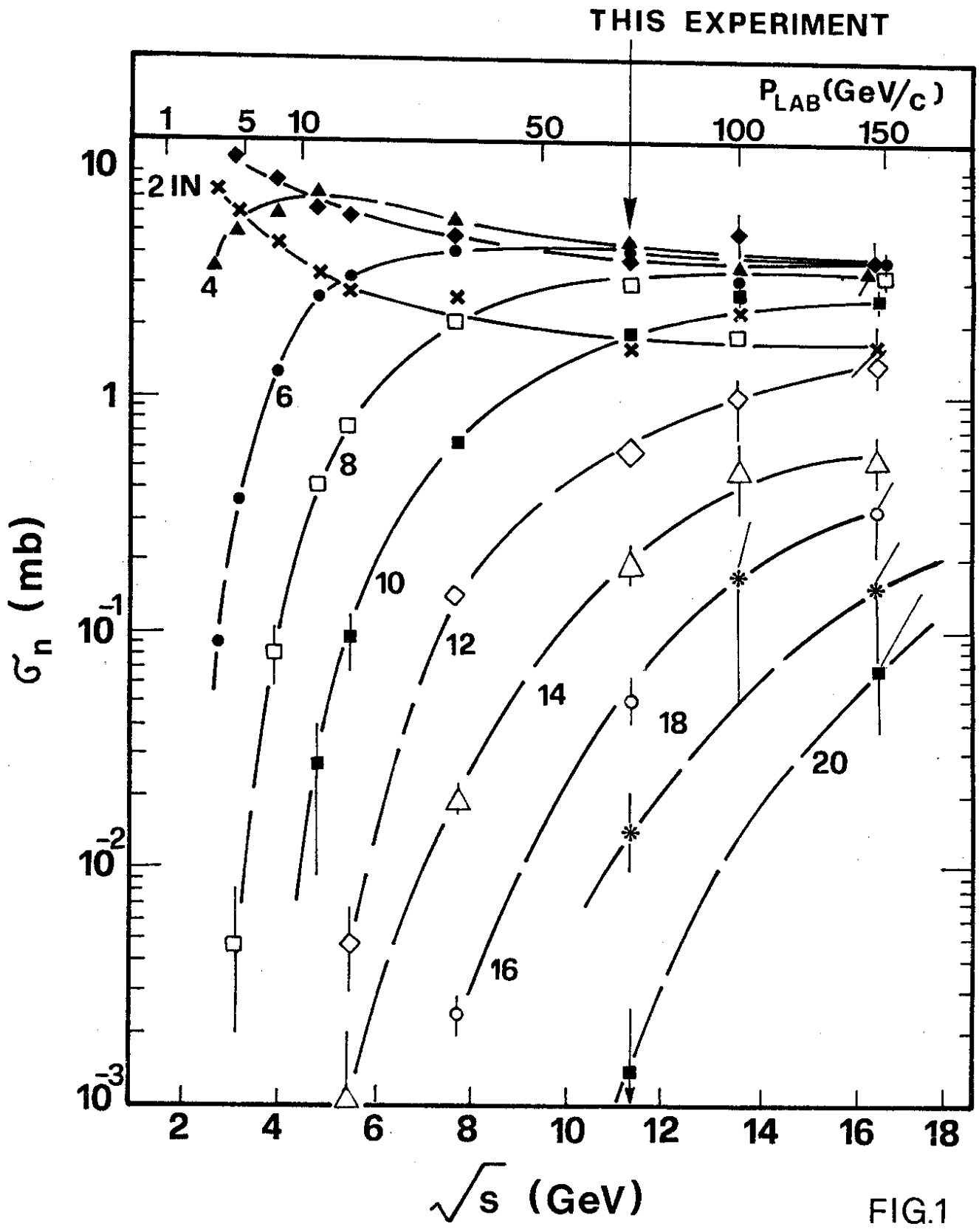
THIS EXPERIMENT
P_{LAB}(GeV/c)
1
5
10
50
100
150
10
1
10^{-1}
10^{-2}
10^{-3}
σ_n (mb)
2 IN
4
6
8
10
12
14
16
18
20
2
4
6
8
10
12
14
16
18
$\sqrt{s}$ (GeV)

FIG.1

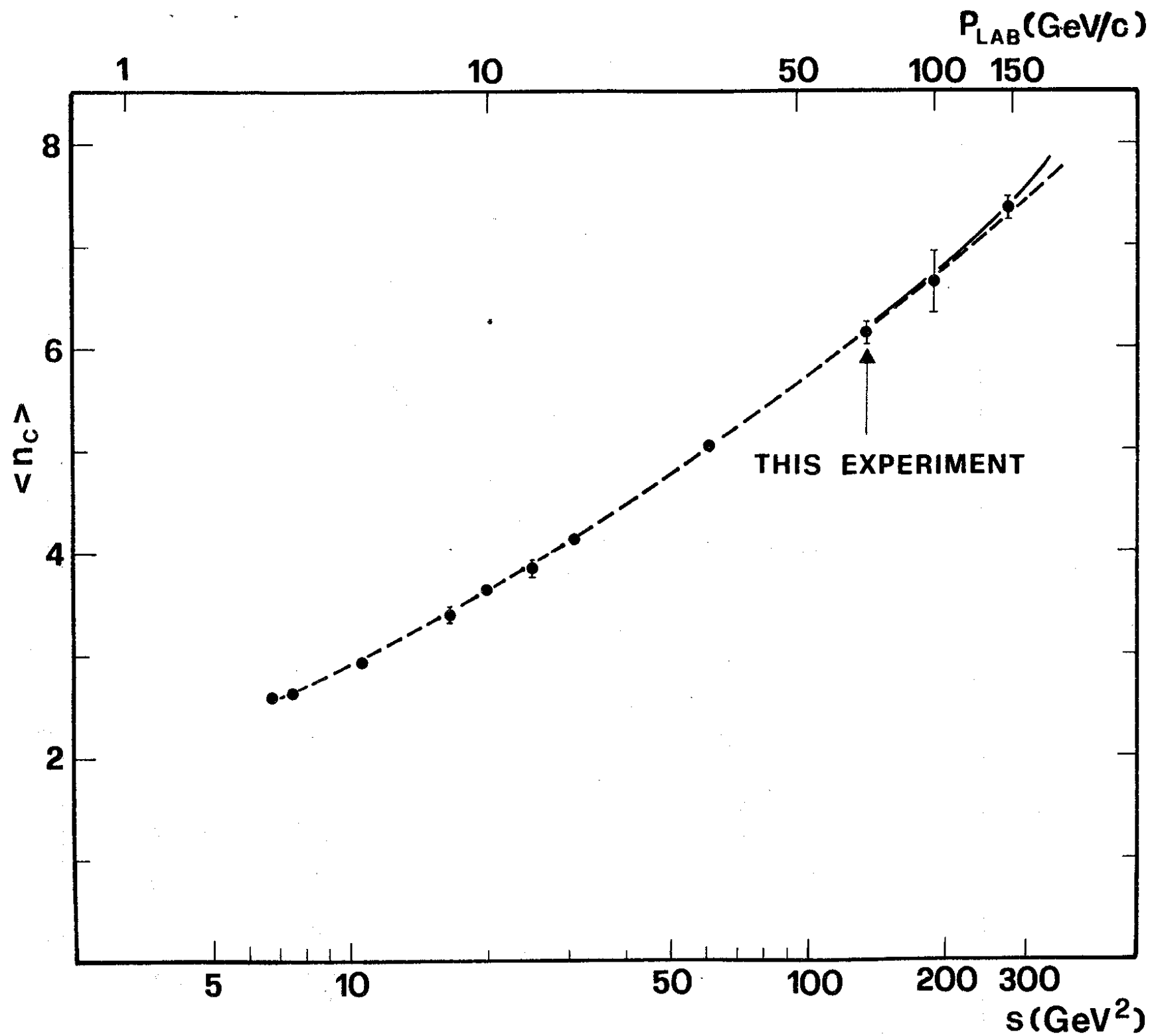
P_{LAB}(GeV/c)
1
10
50
100
150
8
6
4
2
$\langle n_c \rangle$
THIS EXPERIMENT
5
10
50
100
200
300
s(GeV^2)

FIG. 2

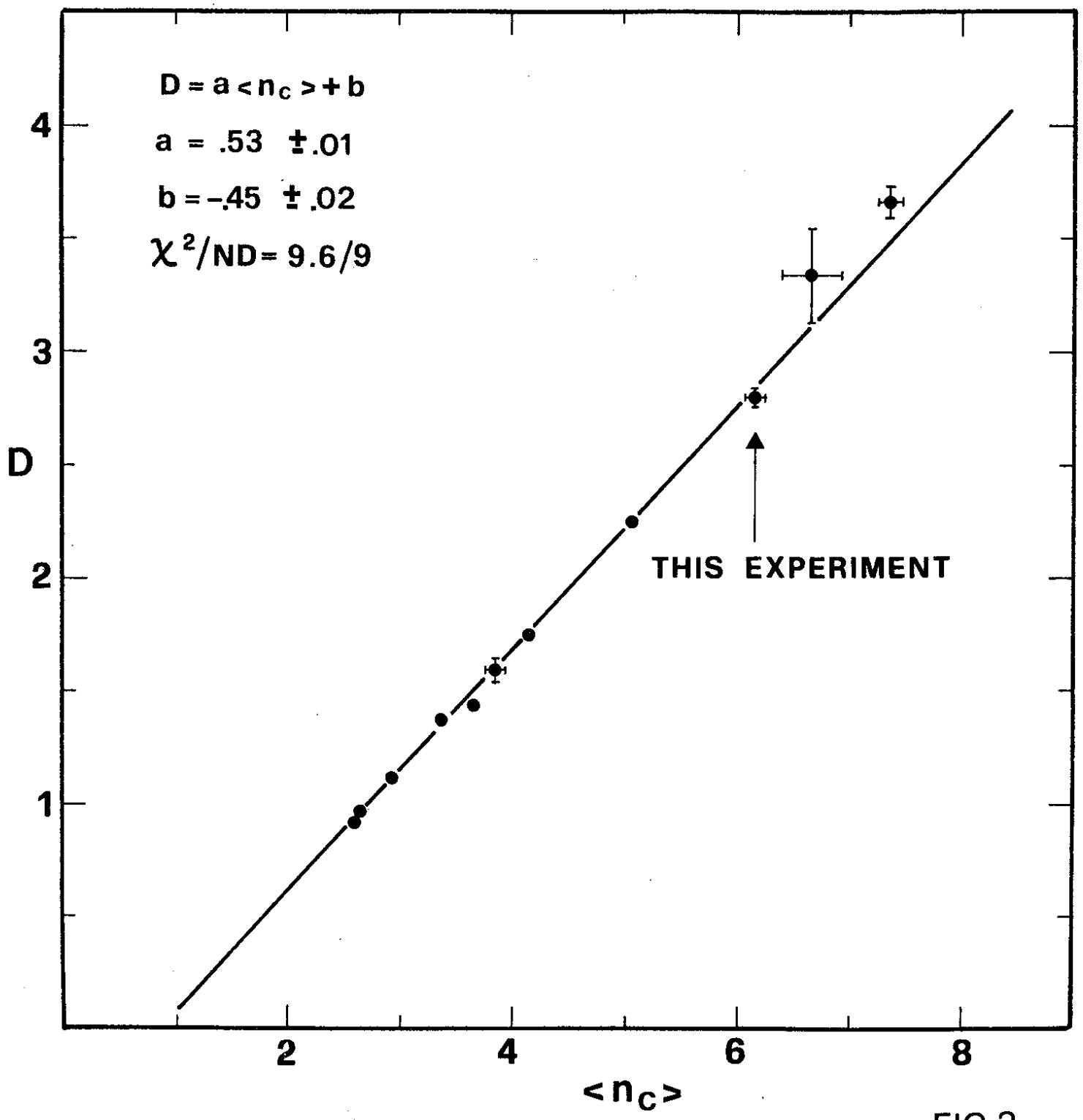

FIG.3

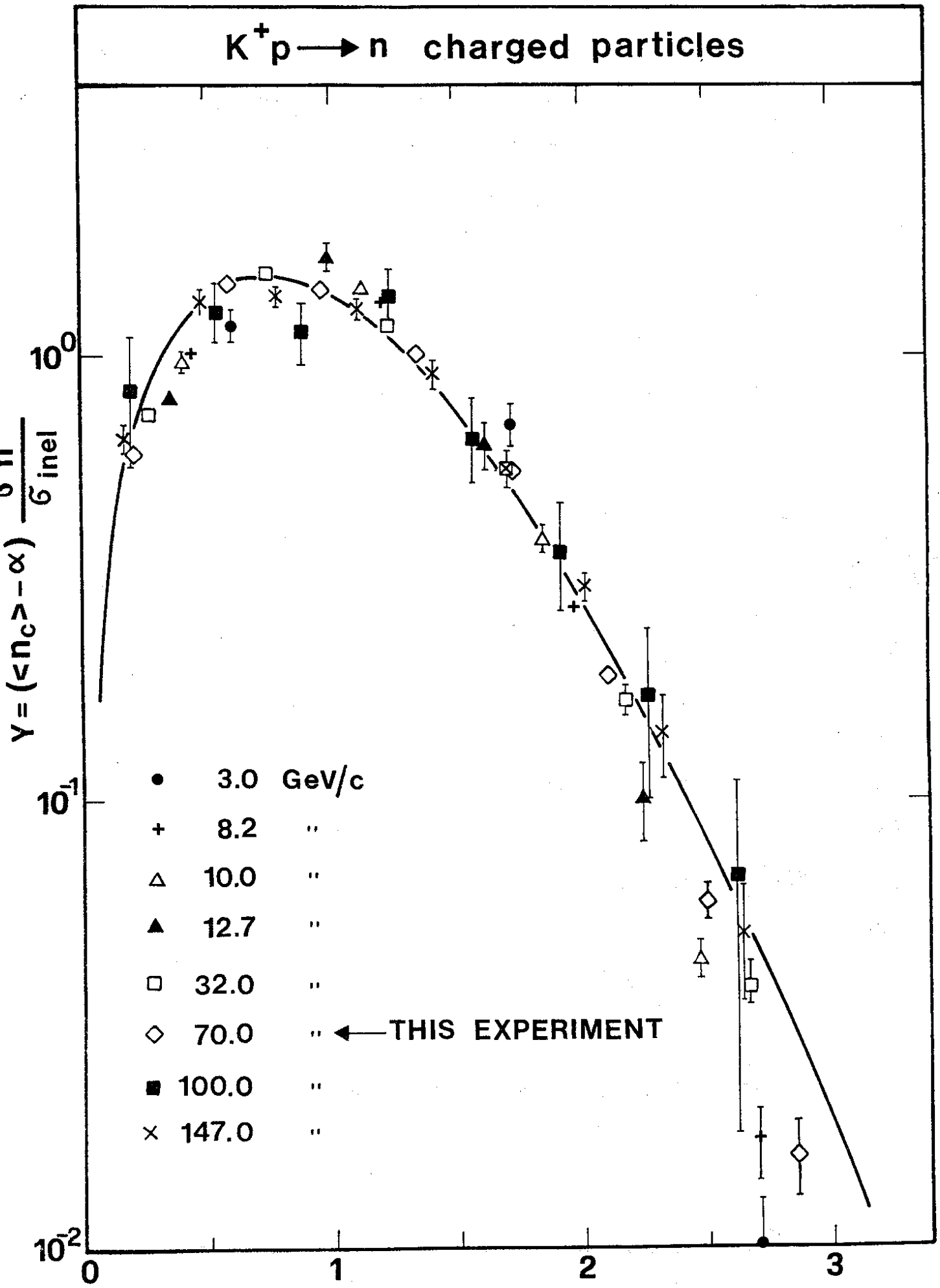
$K^+p \longrightarrow n$ charged particles
$Y = (\langle n_c \rangle - \alpha) \frac{\sigma n}{\sigma_{inel}}$
10^0
10^{-1}
10^{-2}
0
1
2
3
3.0 GeV/c
8.2 "
10.0 "
12.7 "
32.0 "
70.0 " ← THIS EXPERIMENT
100.0 "
147.0 "
$z = \frac{n_c - \alpha}{\langle n_c \rangle - \alpha}$

FIG. 4a

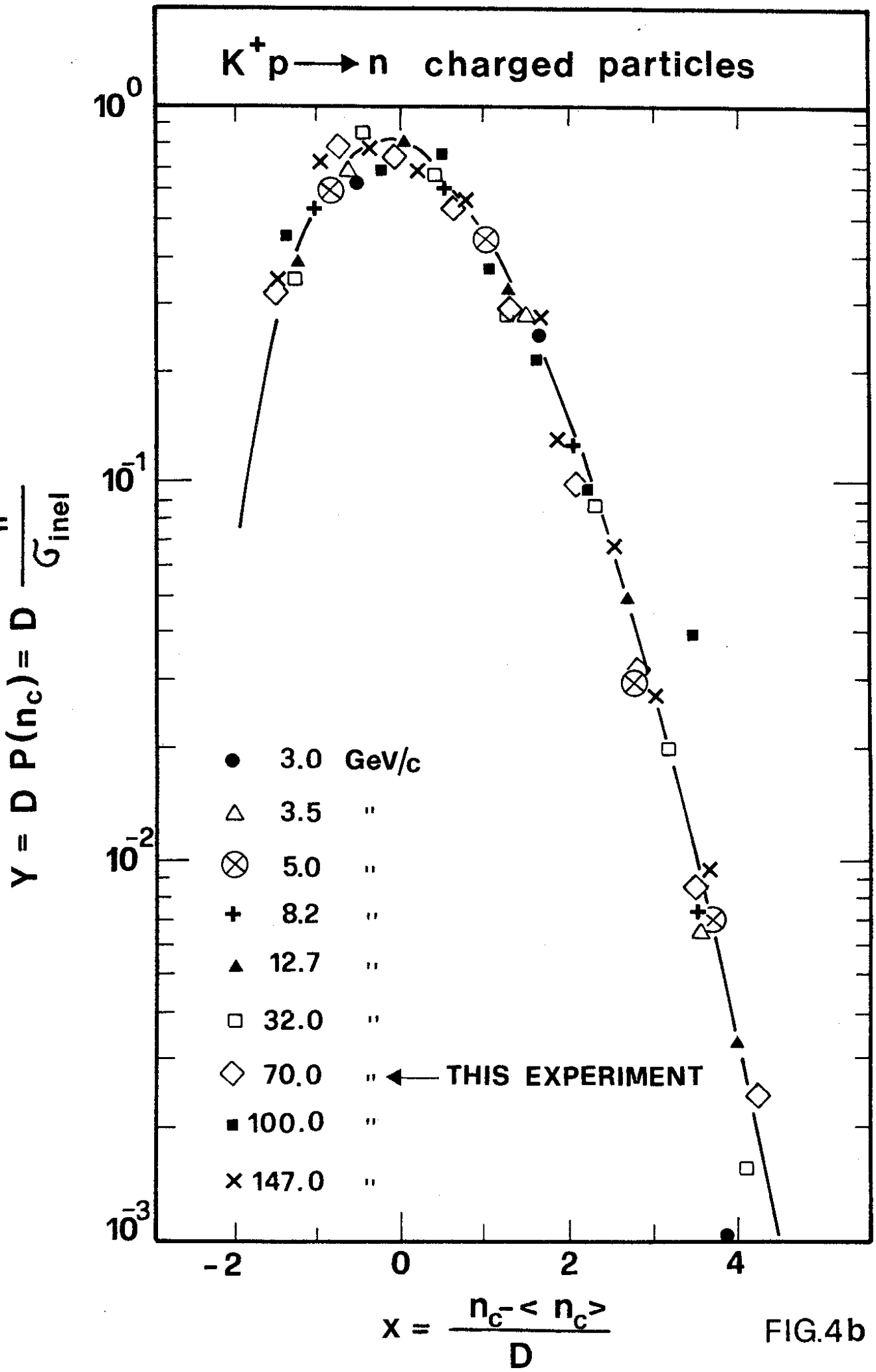
$K^+p \longrightarrow n$ charged particles
$Y = D\,P(n_c) = D\,\frac{\sigma_n}{\sigma_{inel}}$
10^0
10^{-1}
10^{-2}
10^{-3}
3.0 GeV/c
3.5 "
5.0 "
8.2 "
12.7 "
32.0 "
70.0 " ← THIS EXPERIMENT
100.0 "
147.0 "
-2
0
2
4
$x = \frac{n_c - \langle n_c \rangle}{D}$

FIG.4b

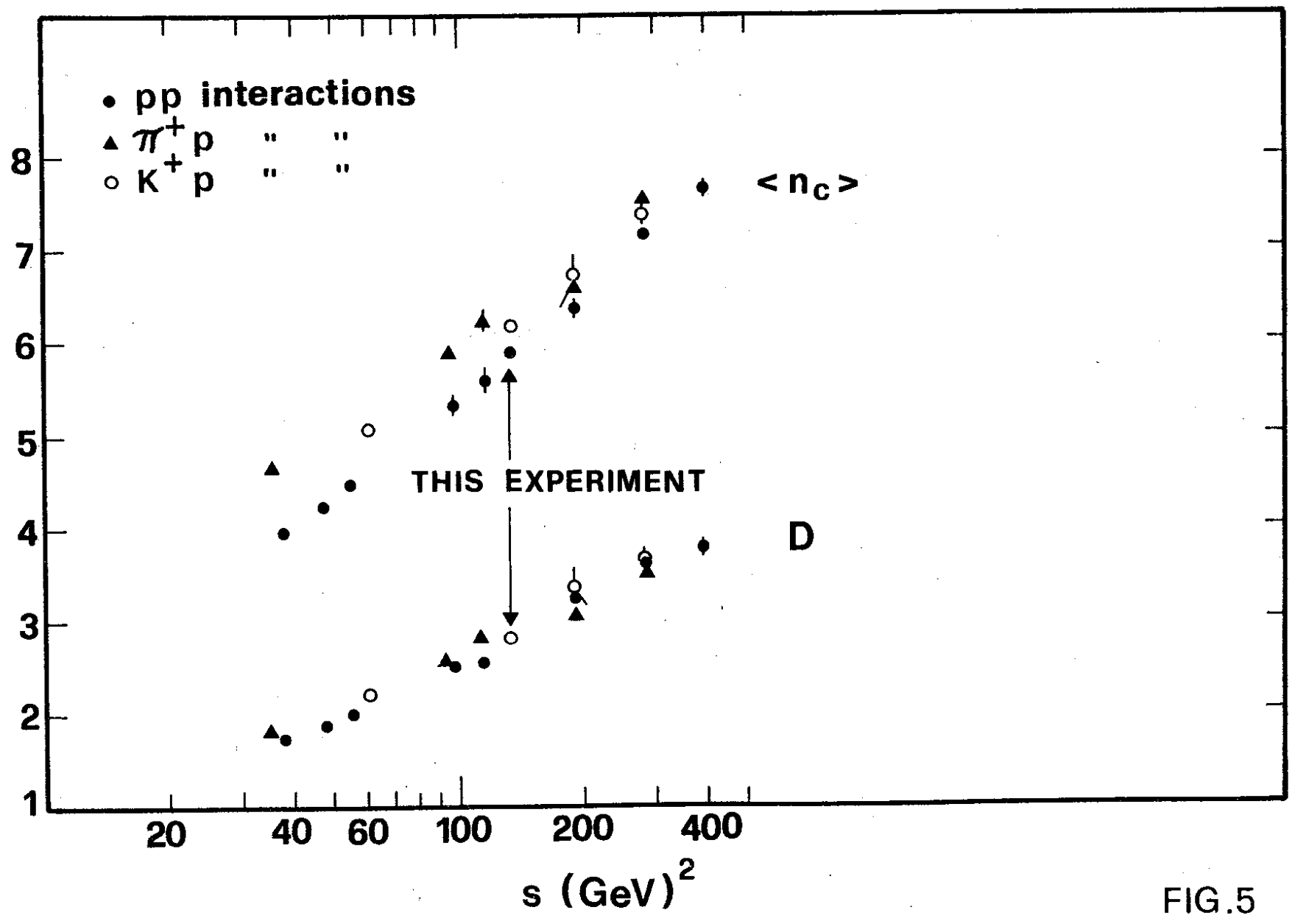
• pp interactions
▲ π+ p " "
○ K+ p " "
< nc >
D
THIS EXPERIMENT
8
7
6
5
4
3
2
1
20
40
60
100
200
400
s (GeV)2

FIG.5

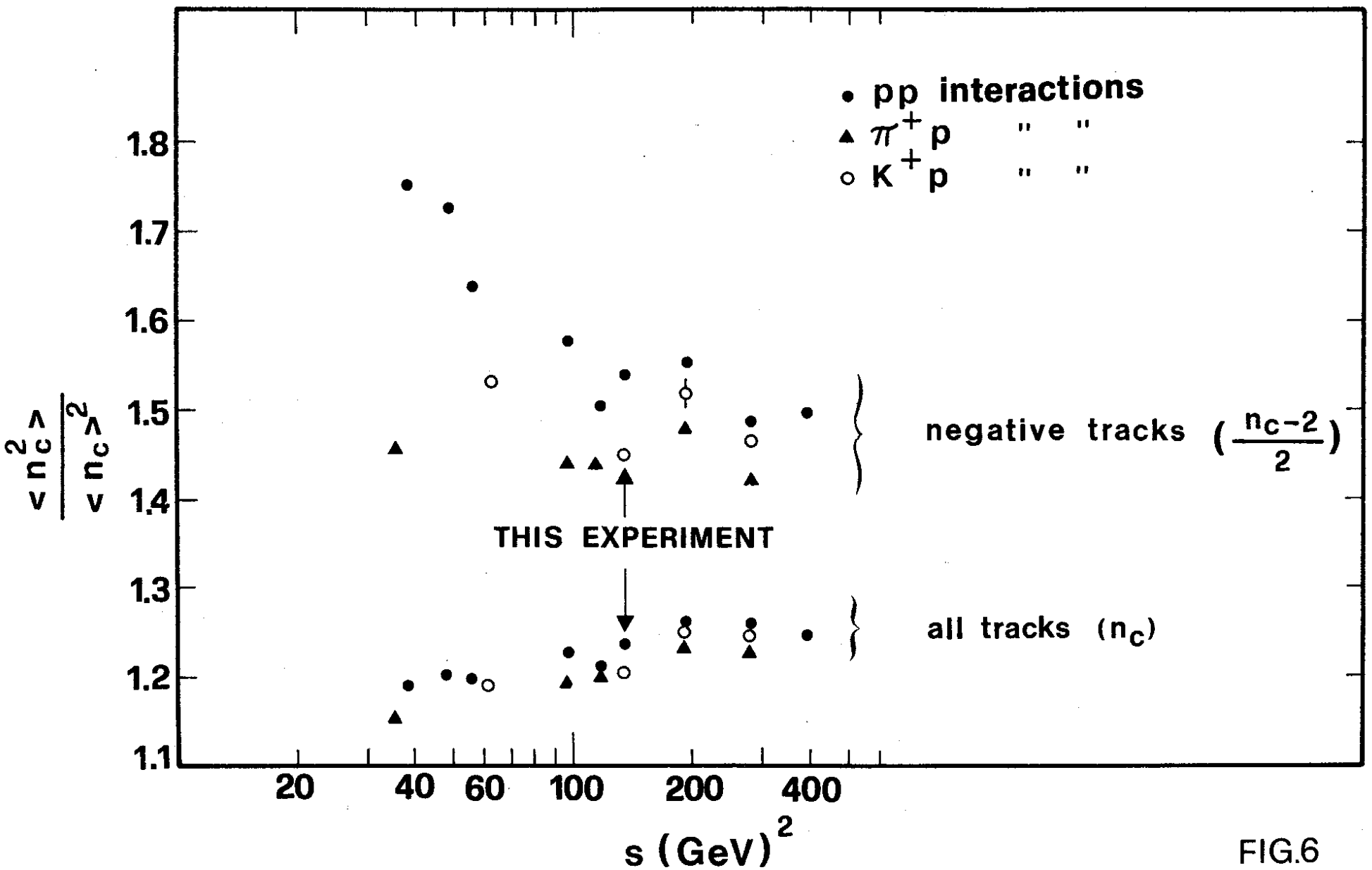
pp interactions
π^+p " "
K^+p " "
negative tracks $(\frac{n_c-2}{2})$
all tracks (n_c)
THIS EXPERIMENT
$\frac{\sqrt{\langle n_c^2\rangle}}{\langle n_c\rangle}$
1.8
1.7
1.6
1.5
1.4
1.3
1.2
1.1
20
40
60
100
200
400
s (GeV)^2

FIG.6

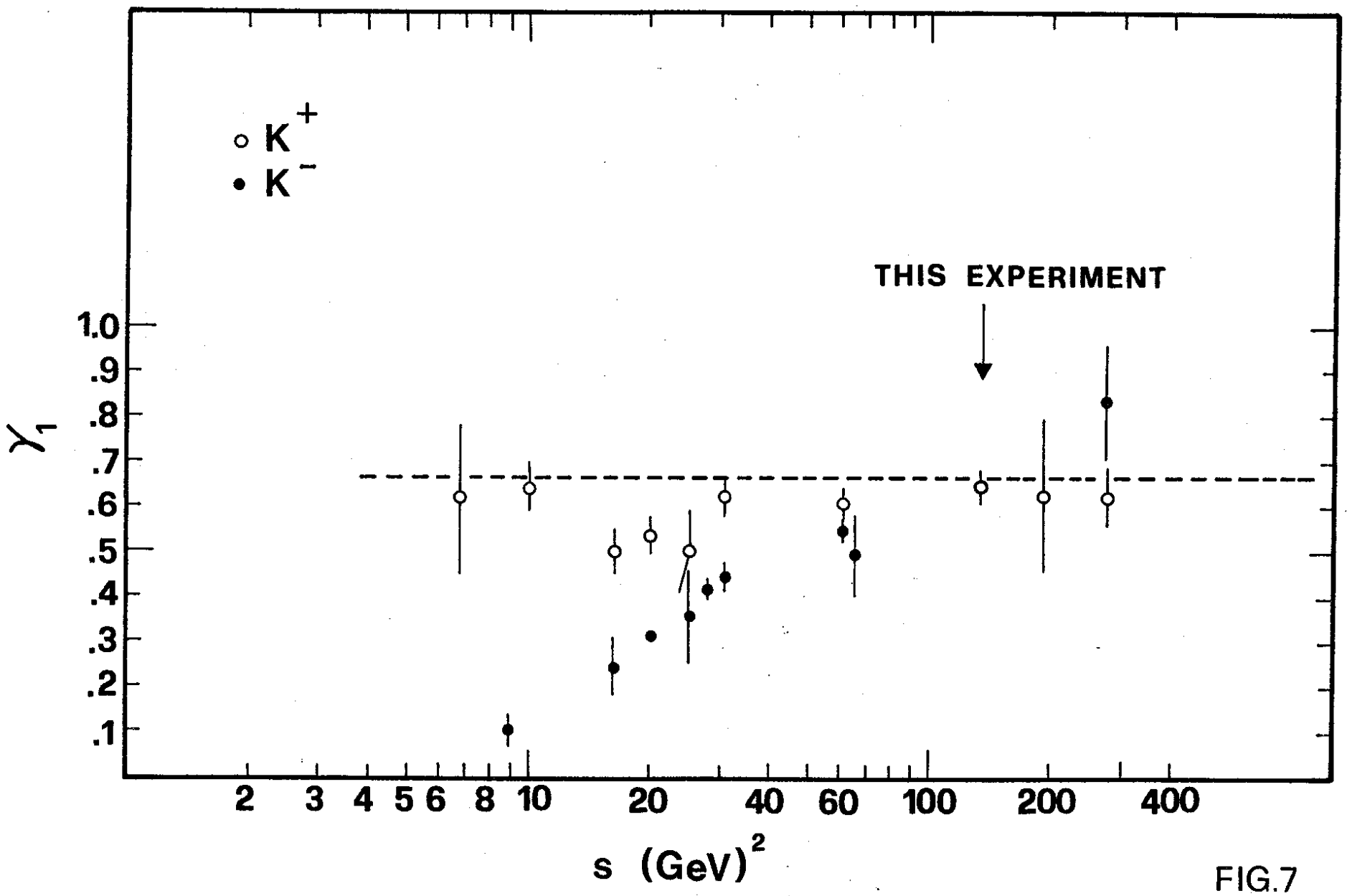
$\circ$ K^+
$\bullet$ K^-
THIS EXPERIMENT
γ_1
1.0
.9
.8
.7
.6
.5
.4
.3
.2
.1
2
3
4
5
6
8
10
20
40
60
100
200
400
s (GeV)^2

FIG.7

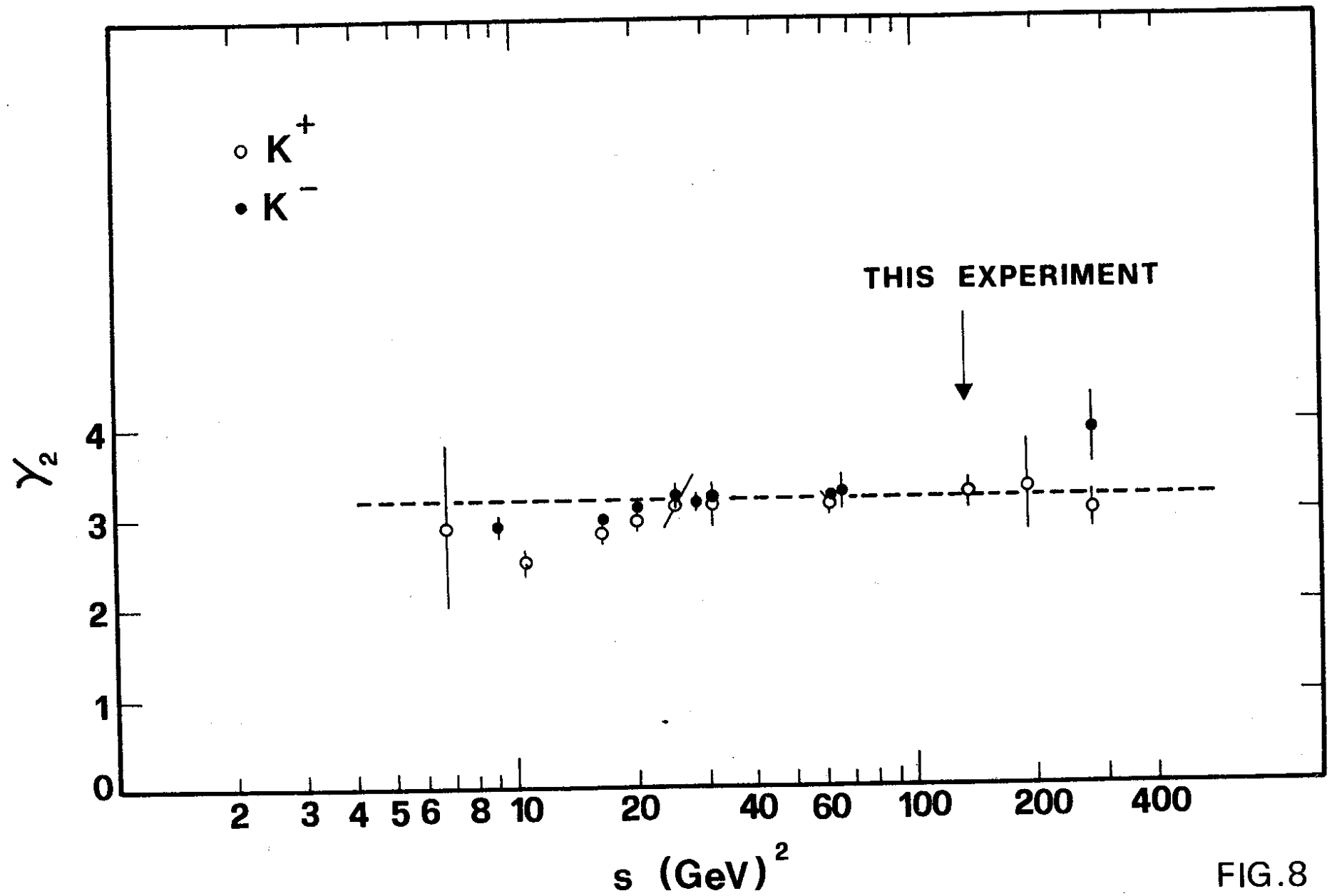
$\circ$ K^+
$\bullet$ K^-
THIS EXPERIMENT
γ_2
0
1
2
3
4
2
3
4
5
6
8
10
20
40
60
100
200
400
s (GeV)^2

FIG.8

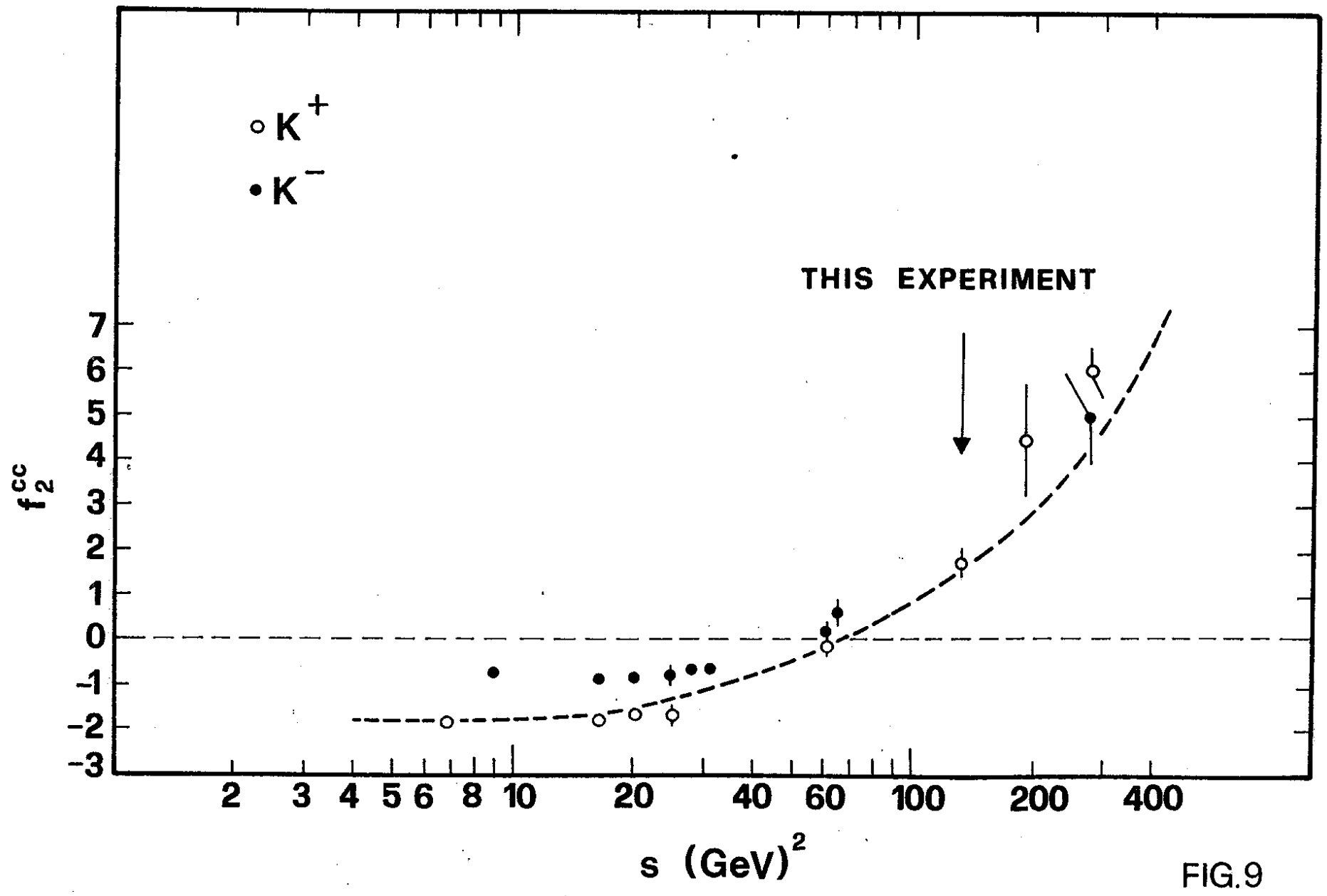
$\circ K^+$
$\bullet K^-$
THIS EXPERIMENT
f_2^{cc}
7
6
5
4
3
2
1
0
−1
−2
−3
2
3
4
5
6
8
10
20
40
60
100
200
400
s (GeV)^2

FIG.9

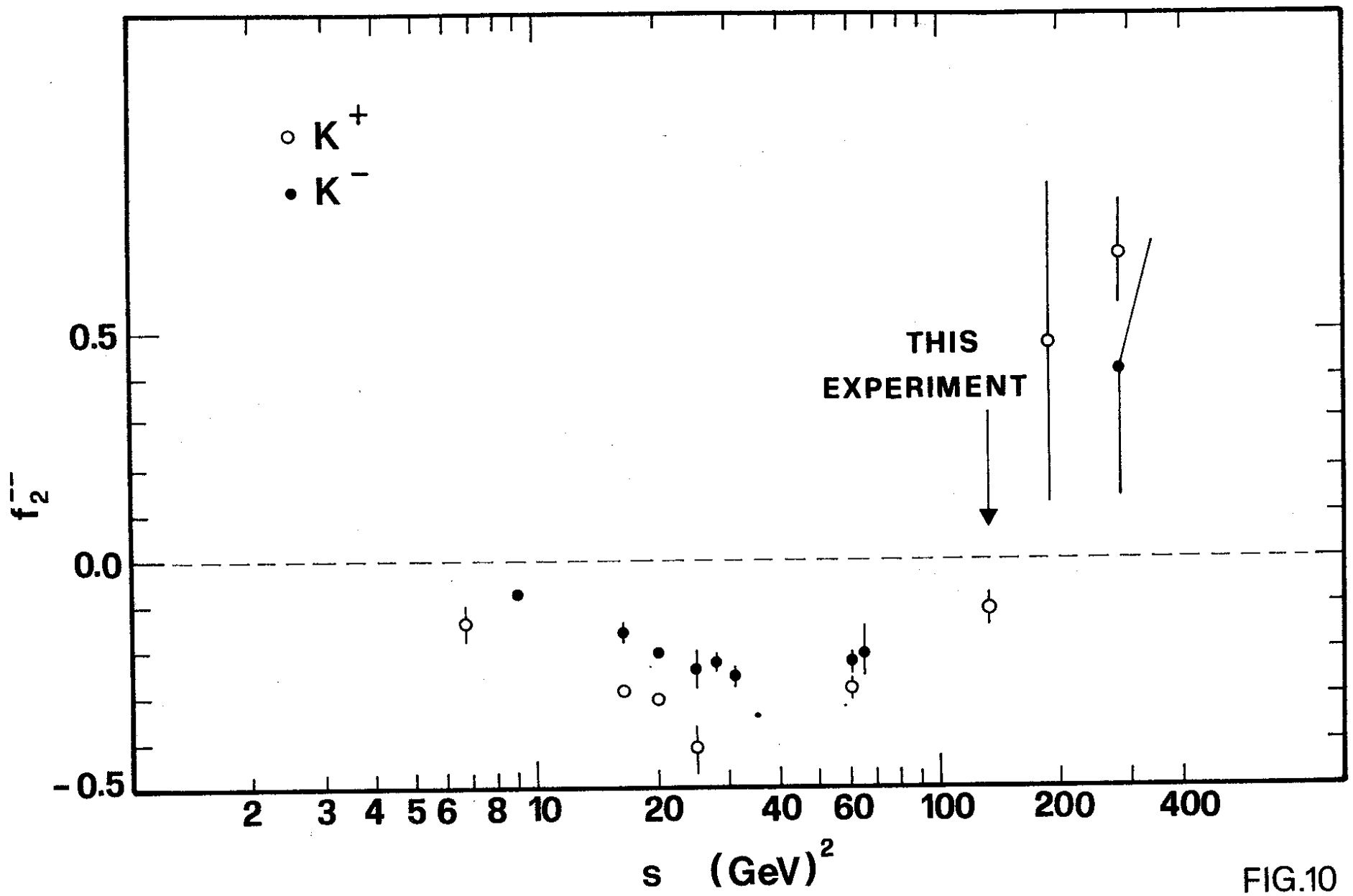
○ K+
• K−
THIS
EXPERIMENT
0.5
0.0
−0.5
f2−−
2
3
4
5
6
8
10
20
40
60
100
200
400
s (GeV)2

FIG.10